Fission yeast tropomyosin specifies directed transport of myosin-V along actin cables

Joseph E. Clayton, Luther W. Pollard, Maria Sckolnick, Carol S. Bookwalter, Alex R. Hodges*, Kathleen M. Trybus, and Matthew Lord
Department of Molecular Physiology and Biophysics, University of Vermont, Burlington, VT 05405

ABSTRACT **A hallmark of class-V myosins is their processivity—the ability to take multiple steps along actin filaments without dissociating. Our previous work suggested, however, that the fission yeast myosin-V (Myo52p) is a nonprocessive motor whose activity is enhanced by tropomyosin (Cdc8p). Here we investigate the molecular mechanism and physiological relevance of tropomyosin-mediated regulation of Myo52p transport, using a combination of in vitro and in vivo approaches. Single molecules of Myo52p, visualized by total internal reflection fluorescence microscopy, moved processively only when Cdc8p was present on actin filaments. Small ensembles of Myo52p bound to a quantum dot, mimicking the number of motors bound to physiological cargo, also required Cdc8p for continuous motion. Although a truncated form of Myo52p that lacked a cargo-binding domain failed to support function in vivo, it still underwent actin-dependent movement to polarized growth sites. This result suggests that truncated Myo52p lacking cargo, or single molecules of wild-type Myo52p with small cargoes, can undergo processive movement along actin-Cdc8p cables in vivo. Our findings outline a mechanism by which tropomyosin facilitates sorting of transport to specific actin tracks within the cell by switching on myosin processivity.**

Monitoring Editor
Laurent Blanchoin
CEA Grenoble

Received: Apr 17, 2013
Revised: Oct 28, 2013
Accepted: Oct 30, 2013

INTRODUCTION

The myosin motors are large, actin-activated ATPases that use the free energy generated from P_i release to power conformational changes leading to contractility, tension, or transport. Tropomyosins, on the other hand, are small, dimeric, α-helical coiled-coil proteins that bind end to end along both sides of the actin filament (Gunning *et al.*, 2005). Tropomyosin promotes actin filament stability and has long been known to work in concert with the troponin complex to regulate striated muscle myosin-II motors by gating access to the actin track in a calcium-dependent manner (Cooper, 2002; Gunning *et al.*, 2005). Whereas troponin is unique to muscle, tropomyosin is widespread, yet exactly how this protein influences myosins in nonmuscle systems is not clear. There is a vexing number of possibilities with respect to actomyosin regulation when one considers the abundance of tropomyosin and myosin isoforms in mammalian cells. Humans use four tropomyosin genes to generate >40 tropomyosin isoforms by alternative splicing, and there are at least 10 classes of myosin motors in humans, each with multiple isoforms.

Fission yeast provides an excellent model system with which to probe the role of tropomyosin in nonmuscle myosin regulation. Cdc8p is the sole tropomyosin, which is essential for the formation of the actomyosin contractile ring and the actin cables spanning the length of the cell (Balasubramanian *et al.*, 1992). Moreover, only three classes of myosins (I, II, and V) are represented in fission yeast. We recently showed that Cdc8p promotes myosin-II activity and actomyosin ring assembly during cytokinesis (Stark *et al.*, 2010). This same regulation may account for the ability of tropomyosins to enhance the activity of smooth muscle myosin-II and platelet myosin-II (myosin-IIA) observed in past studies (Nosaka *et al.*, 1984; Yamaguchi *et al.*, 1984; Merkel *et al.*, 1989). Cdc8p also regulates unconventional myosins from fission yeast (Clayton *et al.*, 2010). Decoration of actin filaments with Cdc8p inhibited myosin-I (Myo1p) but enhanced

This article was published online ahead of print in MBoC in Press (http://www.molbiolcell.org/cgi/doi/10.1091/mbc.E13-04-0200) on November 6, 2013.

*Present address: Department of Chemistry and Physical Sciences, Quinnipiac University, Hamden, CT 06518.

Address correspondence to: Matthew Lord (matthew.lord@uvm.edu), Kathleen M. Trybus (kathleen.trybus@uvm.edu).

Abbreviations used: GFP, green fluorescent protein; Qdot, quantum dot; *Sc* Myo2p, class V myosin from *Saccharomyces cerevisiae*; *Sp* Myo2p, class II myosin from *Schizosaccharomyces pombe*; TIRF, total internal reflection fluorescence.

© 2014 Clayton *et al.* This article is distributed by The American Society for Cell Biology under license from the author(s). Two months after publication it is available to the public under an Attribution–Noncommercial–Share Alike 3.0 Unported Creative Commons License (http://creativecommons.org/licenses/by-nc-sa/3.0).

"ASCB®," "The American Society for Cell Biology®," and "Molecular Biology of the Cell®" are registered trademarks of The American Society of Cell Biology.

the activity of the myosin-Vs (Myo51p and Myo52p). The ability of Cdc8p to inhibit Myo1p is consistent with studies showing that tropomyosin can block myosin-I activity in higher eukaryotes (Collins *et al.*, 1990; Fanning *et al.*, 1994; Tang and Ostap, 2001). However, the ability of Cdc8p to promote Myo51p and Myo52p activity was the first example of tropomyosin-mediated regulation of a class V myosin.

Most myosin-V isoforms studied to date are high–duty ratio motors, meaning that they spend a large proportion of their ATPase cycle in the strong actin-bound ADP or apo states. The high duty ratio and dimeric nature of such motors facilitates processive, hand-over-hand walking along actin filaments (De La Cruz *et al.*, 1999; Mehta *et al.*, 1999). Recent kinetic and motility studies suggest, however, that a subpopulation of myosin-V isoforms are low–duty ratio motors. These include class V myosin from the budding yeast *Saccharomyces cerevisiae* (*Sc* Myo2p; Reck-Peterson *et al.*, 2001), *Drosophila* myosin-V (Toth *et al.*, 2005), human myosin-Vc (Takagi *et al.*, 2008; Watanabe *et al.*, 2008), and fission yeast Myo52p (Clayton *et al.*, 2010). Using single-molecule techniques, we recently confirmed that *Sc* Myo2p is not processive on bare actin but, surprisingly, becomes highly processive when it walks on actin-tropomyosin. Tropomyosin increases the time the motor spends strongly attached to actin by slowing the rate of Mg^{2+}-ADP release. This is the first example of tropomyosin switching a motor from nonprocessive to processive motion (Hodges *et al.*, 2012).

Here we used single-molecule approaches and total internal reflection fluorescence (TIRF) microscopy to show that decoration of actin by Cdc8p also converts single molecules of fission yeast Myo52p into processive motors. In vitro results suggest a mechanism involving both kinetic and cooperative regulation of actomyosin interactions by tropomyosin-actin. Our findings have physiological relevance because truncated Myo52p, lacking its cargo-binding domain (and thus presumably operating as a single molecule), can still undergo directed motility along actin cables in the cell. Of importance, small ensembles of Myo52p motors that support directed transport in vivo also relied on tropomyosin to support motility when reconstituted in vitro. We propose that tropomyosins can sort myosin molecules to specific actin populations by programming a switch from nonprocessive to processive behavior.

RESULTS

Fission yeast tropomyosin converts Myo52p into a processive motor

We tested whether Myo52p was processive or not using single-molecule assays. Our previous duty ratio estimates (percentage of time a motor spends in the strong actin-bound ADP/apo state per ATPase hydrolysis cycle), calculated from actin-activated ATPase and ensemble motility data, suggested that Myo52p comes up well short of being processive even in the presence of tropomyosin (Clayton *et al.*, 2010). A minimum duty ratio of 50% is required for processive stepping of a myosin-V dimer along an actin filament. To examine this question further, we coexpressed a truncated heavy meromyosin (HMM) form of Myo52p, which lacks the C-terminal cargo-binding globular tail domain, with the Myo52p light chains Cam1p (calmodulin) and Cdc4p (essential light chain) in the baculovirus-Sf9 insect cell system (Figure 1A). The Myo52p-HMM had a C-terminal biotin tag for attachment to streptavidin–quantum dots (Qdots) or a streptavidin-conjugated fluorophore (Figure 1A) and a FLAG tag to facilitate affinity purification (Figure 1, A and B).

TIRF microscopy was used to determine whether single Myo52p motors were able to walk processively along actin filaments. Fluorescently labeled actin filaments were attached to a glass coverslip,

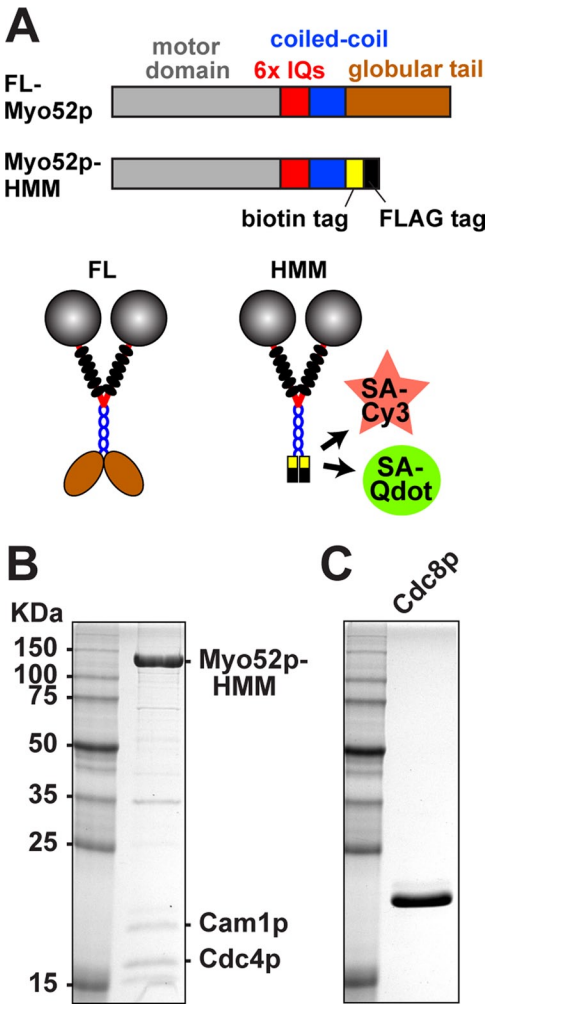

FIGURE 1: Myo52p constructs and purification. (A) Top, linear representations of full-length and truncated Myo52p constructs. The positions of specific domains are indicated on the full-length construct. Truncated Myo52p-HMM (amino acids 1–1056 of the Myo52p heavy chain) was used in TIRF-based motility assays. This construct contains a biotin tag following the coiled-coil for attachment to streptavidin-coated Qdots or streptavidin-Cy3, and a FLAG tag to facilitate affinity purification. The C-terminus of both full-length and truncated forms of Myo52p were fused to triple GFP for in vivo studies (Figures 4–6). Bottom, corresponding illustrations of double-headed Myo52p molecules. Six light chains (black ovals) bind to the IQ region of each Myo52p polypeptide. (B, C) Purified protein samples after SDS–PAGE and gel staining with Coomassie blue. Molecular weight standards are included in the left lanes. (B) Myo52p-HMM after elution from anti-FLAG purification resin. HMM was co-overexpressed with its two (untagged) light chains: Cam1p and Cdc4p. These light chains were also purified independently (see *Materials and Methods*) and added to HMM samples at 10-fold molar excess to minimize light-chain dissociation and suboptimal Myo52p motor activity in biochemical assays. (C) Fission yeast tropomyosin Cdc8p was purified from bacteria as an acetylated-mimicking form.

and a solution containing Myo52p labeled with fluorescent quantum dots was added. No processive movements were observed (Supplemental Movie S1), suggesting that Myo52p has a duty ratio <50% on bare actin under our in vitro conditions. On the basis of the observation that budding yeast myosin-V (*Sc* Myo2p) requires tropomyosin for processivity, and because the actin cables on which

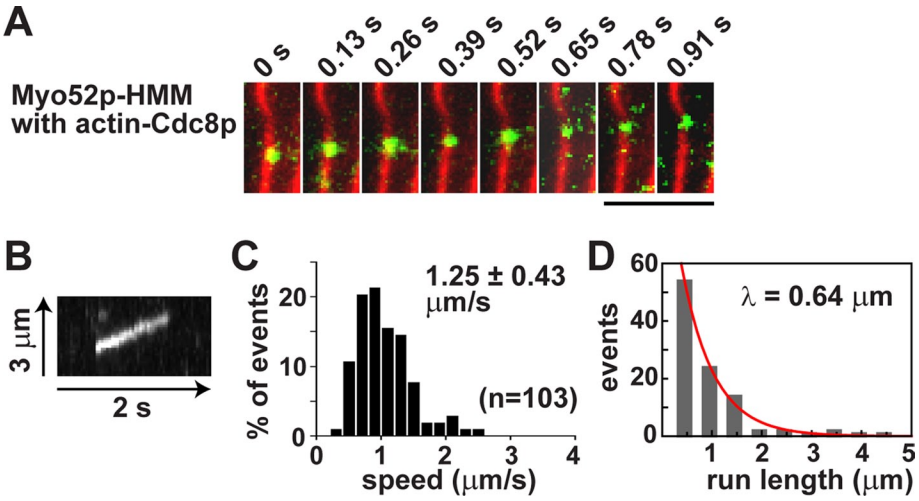

FIGURE 2: Fission yeast tropomyosin is required for transport of single Myo52p molecules along actin filaments. Processive movement of Myo52p-HMM molecules coupled to Qdots (1:10 M ratio) along rhodamine-phalloidin–labeled actin filaments using TIRF microscopy. (A) Movement of a Myo52p-Qdot (green) along a Cdc8p-decorated actin filament (red). Bar, 4 μm. Other representative events are presented in Supplemental Movie S1. (B) Kymograph showing a typical Myo52p-Qdot run along an actin-Cdc8p filament. (C) Histogram of the speed distribution of Myo52p-Qdots. (D) Run length histogram of Myo52p-Qdots moving on Cdc8p-actin tracks. The red curve shows the exponential fit ($y = Ae^{-x/\lambda}$), which yields the run length λ.

Myo52p transports cargo in the cell depend on Cdc8p for their assembly and maintenance (Balasubramanian *et al.*, 1992; Arai *et al.*, 1998), we repeated these experiments using Cdc8p-decorated filaments. Recombinant Cdc8p was purified from bacteria (Figure 1C). Strikingly, the presence of Cdc8p facilitated processive movements of Myo52p– quantum dots (Qdots) along actin filaments (Figure 2, A and B, and Supplemental Movie S1). The switch in behavior was quite dramatic, given that the processive runs showed efficiency in terms of both speed (~1.25 μm/s; Figure 2C) and run length (~0.6 μm; Figure 2D), values comparable to those for bona fide processive myosin-Vs previously characterized using this approach (Warshaw *et al.*, 2005). The experiments were repeated using Myo52p labeled with a streptavidin-Cy3 fluorescent dye instead of quantum dots. The Cy3-labeled Myo52p molecules moved processively only when actin filaments were decorated with Cdc8p (Supplemental Figure S1 and Supplemental Movie S2). We assume that both of our labeling approaches achieve single-molecule resolution, thereby demonstrating that tropomyosin is required for Myo52p to move processively.

Tropomyosin increases Myo52p run frequency and run length at low ATP concentration

The ability of tropomyosins to activate Myo52p processivity suggests that tropomyosin may increase the duty ratio of the motor by increasing the occupancy of the strong actin-bound ADP or apo states. To further understand the mechanism by which Cdc8p contributes to Myo52p processivity, we repeated our single-molecule studies at low (10 μm) ATP. At this concentration ATP binding becomes the rate-limiting step of the Myo52p ATPase cycle, allowing the strongly bound apo state to predominate. Thus the nonphysiological low ATP concentration increases the duty ratio, and Myo52p remains strongly bound to actin as it awaits an ATP molecule to bind and dissociate the head from actin.

Under these low-ATP conditions, Myo52p exhibited processive movements along both bare and Cdc8p-decorated actin filaments (Supplemental Movie S3). Thus Cdc8p becomes dispensable for processivity when the Myo52p duty ratio is artificially increased, similar to what was observed with *Sc* Myo2p from budding yeast and its cognate tropomyosin, Tpm1p (Hodges *et al.*, 2012). Although the speeds of these Myo52p movements were not statistically different on actin versus actin-Cdc8p tracks (Figure 3A), as expected they were more than 10-fold lower than those observed on actin-Cdc8p filaments at 2 mM ATP (Figure 2C). Surprisingly, the frequency at which these runs were observed was more than sevenfold higher when actin was decorated with Cdc8p (Figure 3B and Supplemental Movie S3). Furthermore, the average run lengths were approximately twofold longer in the presence of Cdc8p (Figure 3C). The increased run frequency and run length with Cdc8p at low ATP highlights that Cdc8p does something beyond enhancing the duty cycle of the motor.

Myo52p motors work in small clusters that rely on tropomyosin for effective transport

Myo52p moves along actin cables to polarized growth sites (Grallert *et al.*, 2007), and the localization of a number of different proteins has been shown to rely on this transport, namely α-glucan synthase Mok1p (Win *et al.*, 2001), synaptobrevin Syb1p (Edamatsu and Toyoshima, 2003), β-1,3-glucan synthase Bgs1p (Mulvihill *et al.*, 2006), chitin synthase Chs2p (Martin-Garcia and Valdivieso, 2006), CLIP-170 homologue Tip1p (Martin-Garcia and Mulvihill, 2009), exocytosis factor Mug33p (Snaith *et al.*, 2011), and GTPase Ypt3p (Lo Presti and Martin, 2011). Whereas Myo52p may well operate as a single molecule to directly transport some of these proteins to the cortex, it probably also works as an ensemble in which multiple motors work together to mediate motility via attachment to a larger cargo, such as the previously characterized Syb1p- or Mug33p-associated vesicles (Edamatsu and Toyoshima, 2003; Snaith *et al.*, 2011).

We used clathrin light chain (Clc1p-3x green fluorescent protein [GFP]) at endocytic patches as a standard to estimate the numbers of Myo52p-3xGFP molecules in particles undergoing directed transport. Clc1p is ideal since its distribution at patches has already been quantified (Sirotkin *et al.*, 2010), and its signal intensity is very similar to Myo52p, enabling accurate extrapolation between the similar-sized Clc1p patches and Myo52p particles. We performed time-lapse analysis of a mixed population of *myo52-3xGFP* and *clc1-3xGFP* cells (Figure 4A). Analysis of the two strains in the same field allowed us to estimate the number of Myo52p molecules per motile particle, which ranged from 4 to 34, with a mean of 12.9 ± 6.7 (Figure 4, B and C). Thus four molecules of Myo52p appear to be enough to support directed transport of cargoes in vivo. However, although an average of 13 molecules may be associated with a given cargo, the number of Myo52p molecules contacting the track at any one time is probably less, given the geometry and size of cargoes such as vesicles. Even if Myo52p-decorated vesicles or organelles became stretched out along the length of the actin cable as they moved along the track, approximately half of the Myo52p molecules would still be out of reach of the track, meaning that an average of six to seven molecules is enough to propagate transport in vivo.

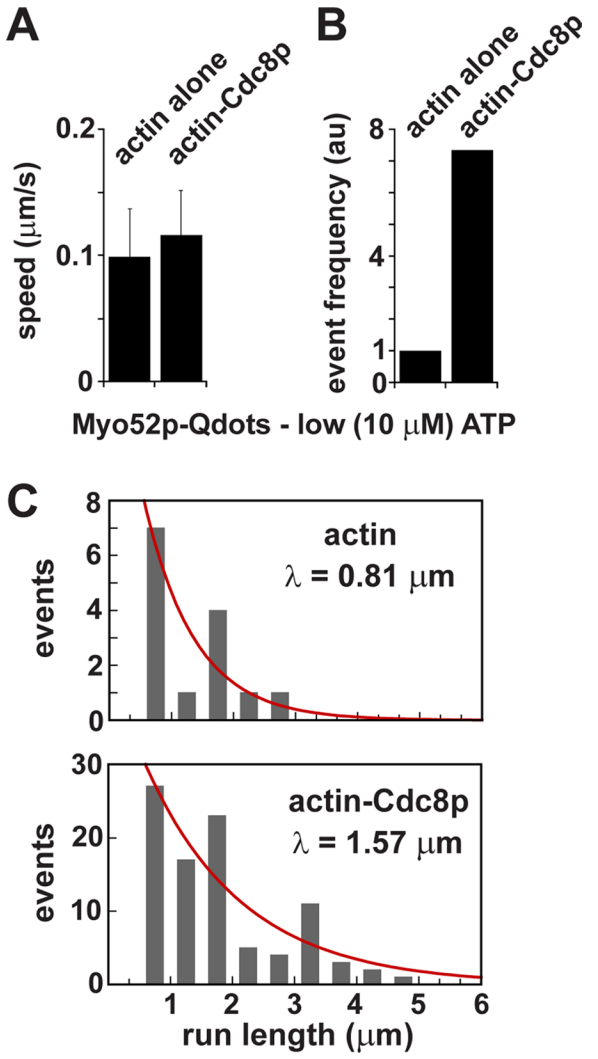

FIGURE 3: Movements of single Myo52p molecules along actin and actin-tropomyosin tracks at low ATP concentration. Processive movement of Myo52p-HMM molecules coupled to Qdots (1:10 M ratio) along rhodamine-phalloidin–labeled actin filaments at low ATP concentration (10 μM) using TIRF microscopy. Representative events are presented in Supplemental Movie S3. (A) Speeds of Myo52p-Qdots on actin vs. actin-Cdc8p tracks ($n = 17$, actin alone; $n = 104$, actin-Cdc8p). (B) Relative frequency of Myo52p runs along actin vs. actin-Cdc8p tracks (17 runs/1123.8 μm available actin vs. 104 runs/959.6 μm available actin-Cdc8p). The frequency of Myo52p movements on actin alone was normalized to 1.0. (C) Histogram of run lengths for Myo52p molecules along actin vs. Cdc8p-decorated actin tracks. The red curves show the exponential fits ($y = Ae^{-x/\lambda}$) used to determine the run length, λ.

The in vitro motility behavior of physiologically relevant numbers of Myo52p molecules was examined in the presence or absence of Cdc8p. Qdots were mixed with a 10-fold molar excess of Myo52p-HMM, yielding approximately three to five molecules per Qdot based on geometrical considerations. As seen at the single-molecule level, bare actin was unable to support transport by multiple Myo52p motors (Supplemental Movie S4). However, Cdc8p-decorated actin filaments supported continuous motility by multiple motors (Supplemental Figure S2A and Supplemental Movie S4). These overloaded Qdots exhibited similar speeds to single Myo52p molecules, and their average run length was ~1.3-fold higher (Supplemental Figure S2B). This modest increase upon overloading the quantum dots suggests that single Myo52p motors are responsible for motility at the limiting molar ratio. Our findings indicate that Cdc8p is essential for Myo52p transport powered by physiological ensembles of motors.

Myo52p molecules lacking a cargo-binding domain undergo continuous motility along actin cables in vivo

To test the importance of cargo binding in Myo52p transport and polarization, we constructed a truncated form of Myo52p in which the C-terminal cargo-binding globular tail domain was replaced with a triple GFP tag (Myo52pΔCBD-3xGFP). The truncated form did not support cellular function, as reflected by morphological defects reminiscent of a *myo52Δ* strain (Figure 5A) and the inability to colocalize with the cargo-associated protein Ypt3p (Supplemental Figure S3). However, despite the loss-of-function phenotype, Myo52pΔCBD could still accumulate at polarized growth sites (Figure 5B).

Time-lapse analysis of live cells revealed that polarization of Myo52pΔCBD stemmed from its ability to undergo directed transport, similar to full-length Myo52p (Figure 6A and Supplemental Movie S5). Analysis of these intracellular movements revealed a slightly slower speed for the truncated form (Figure 6B), whereas the average run length and frequency of the Myo52pΔCBD particle movements were indistinguishable from those of full-length Myo52p (Figure 6, C and D). Although our findings with the truncated form imply that individual Myo52p molecules are capable of intracellular motility when not bound to a cargo, quantitative analysis of Myo52pΔCBD-3xGFP fluorescence intensities estimated an average of 10 truncated Myo52p molecules/motile particle (Figure 6E). Although motile single molecules cannot be resolved amid the background fluorescence of cytoplasmic Myo52pΔCBD-3xGFP, our cellular counts suggest that truncated motors often move together in groups (making them amenable to detection in our setup).

When actin cables were depolymerized by latrunculin A, Myo52pΔCBD-3xGFP showed diffuse fluorescence throughout the cytoplasm, unlike full-length Myo52p-3xGFP, which showed punctuate fluorescence, which presumably reflects clustering on cargoes (Figure 5B). These data suggest that the groups of truncated motors detected by time-lapse microscopy (Figure 6B) are actin dependent and unlikely due to aggregation propagated by either the motor itself or the 3xGFP of the fusion construct. We further verified this by repeating the latrunculin A experiment using an alternative fluorescent protein tag to label Myo52pΔCBD. We wanted to rule out the possibility that the 3xGFP tags specifically favor aggregation and multiple motor-based transport of Myo52pΔCBD when molecules are put into closer contact (i.e., when they bind close by one another along the actin track). We instead used the equally bright tdTomato tag. Like Myo52pΔCBD-3xGFP, Myo52pΔCBD-tdTomato transported to polarized growth sites in an actin-dependent manner, becoming diffuse throughout the cytoplasm upon treatment with latrunculin A (Supplemental Figure S4).

We conclude that actin-tropomyosin cables support processive movements of Myo52pΔCBD molecules. The observation that these movements can be visualized as relatively uniform groups of Myo52p molecules moving in unison may reflect cooperative binding of motors to Cdc8p-decorated cables under physiological conditions.

DISCUSSION

Here we show that adding tropomyosin to the actin filament converts a single molecule of fission yeast myosin-V from a nonprocessive to a processive motor. Tropomyosin also activates continuous

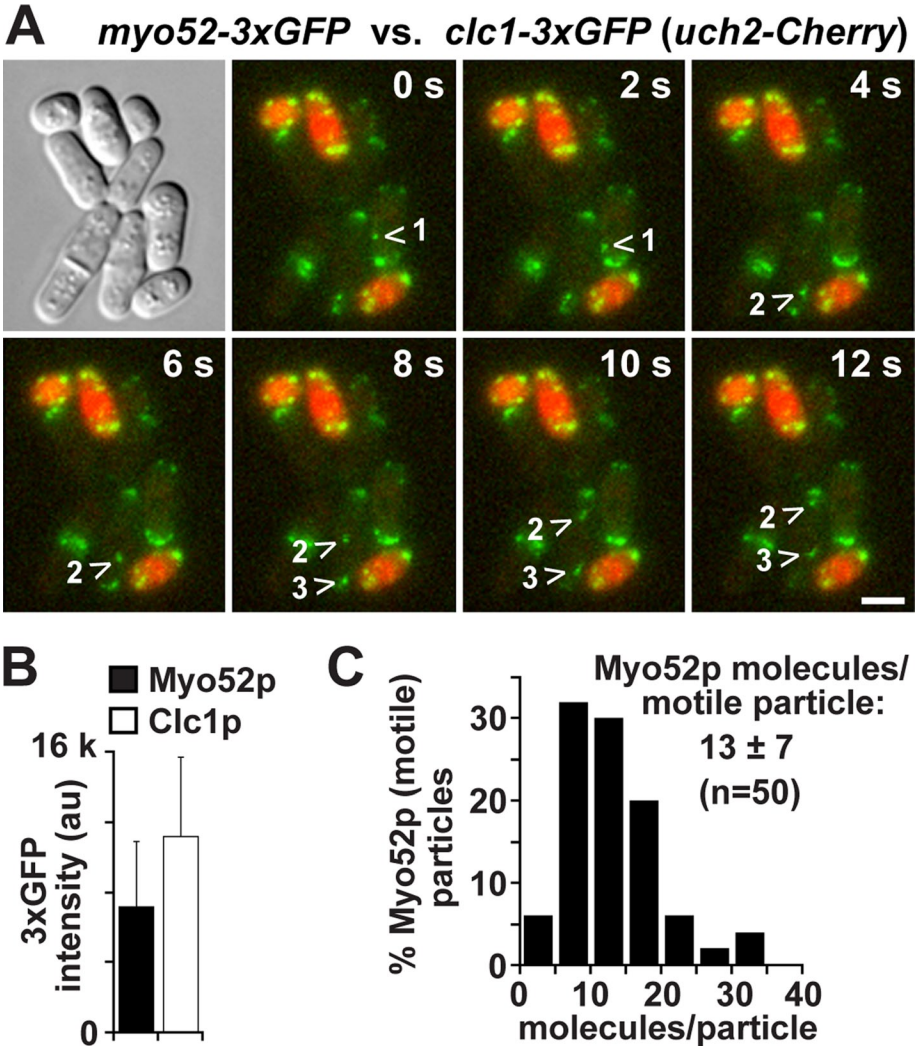

FIGURE 4: Estimating the numbers of Myo52p molecules per motile particle in the cell. The signal intensity of GFP in motile Myo52p-3xGFP particles was used to estimate the number of Myo52p molecules/particle. Clathrin light-chain (Clc1p-3xGFP) signal was used as a standard based on its previously characterized distribution at actin patches (40 molecules/patch; Sirotkin *et al.*, 2010). (A) Representative time-lapse images of a mixed population of *myo52-3xGFP* and *clc1-3xGFP* cells (after growth on YE5S rich medium at 25°C). *clc1-3xGFP* cells were distinguished from *myo52-3xGFP* cells by inclusion of a genomic *uch2-Cherry* fusion, which marks nuclei red. The GFP (green) images shown are maximum projections generated from seven *z*-stacks. The arrowheads track the movement of three different motile Myo52p particles. Bar, 4 μm. (B) Histogram comparing the average GFP intensities for motile Myo52p particles and Clc1p patches. (C) Histogram of the distribution of Myo52p GFP intensities expressed as number of dimeric motors/motile particle.

transport by multiple motors of Myo52p bound to a Qdot. Small ensembles of motors more closely mimic the situation found on cellular cargoes. We determined an average of 13 motors per motile particle in vivo, although this number likely exceeds the number of track-engaged motors at any time. In vivo, Myo52p shows continuous motion along tropomyosin-bound actin cables. Processive motion would ensure highly efficient movement of larger cargoes by multiple Myo52p motors, as well as facilitating transport of cytoplasmic proteins or smaller cargoes by single motors. Whether or not an actin track has tropomyosin bound to it provides a simple mechanism by which myosin motor function can be sorted to specific cellular actin structures (Figure 7). Cdc8p-mediated sorting of Myo52p motors to cables ensures directed transport toward polarized growth sites, as well as contributing to the extension and organization of the cables (Lo Presti *et al.*, 2012), all of which help to establish normal cell shape. This tropomyosin-dependent regulation may be relevant in higher eukaryotes, given that nonprocessive myosin-Vs have also been identified in *Drosophila* and humans (Toth *et al.*, 2005; Takagi *et al.*, 2008; Watanabe *et al.*, 2008).

Tropomyosin promotes Myo52p processivity by altering the kinetics of the motor

Regulation of Myo52p processivity by Cdc8p ultimately involves significant changes in the kinetic properties of the motor. The duty cycle of a processive motor must be >50% to ensure that one head remains strongly bound to actin at any time. The duty cycle can be increased by increasing the time in the strongly bound states or decreasing the time in the weakly bound states. Our previous work with class II myosin from the fission yeast *Schizosaccharomyces pombe* (*Sp* Myo2p) and Myo52p showed that Cdc8p increases the V_{MAX} and apparent actin affinity of these motors in actin-activated ATPase assays while slowing the rates at which they propel actin filaments in filament gliding assays (Clayton *et al.*, 2010; Stark *et al.*, 2010). Given the increased actin affinities and the fact that filament gliding is rate limited by the strong actin-bound state (Siemankowski *et al.*, 1985), the ability of tropomyosin to activate processivity lies in its ability to favor the strong actin-bound state of the actomyosin ATPase cycle, resulting in an increased duty ratio for the motor. The observation that Cdc8p increases Myo52p V_{MAX} values in ATPases (Clayton *et al.*, 2010) suggests that activation of Myo52p processivity may largely involve a significant increase in the rate of P_i release, facilitating rapid movement into the strong actin-bound ADP state.

The detailed effects of tropomyosin depend on the specific myosin isoform. Both Myo52p and budding yeast Myo2p are class V myosins, but they are affected differently by tropomyosin. For Myo2p, steady-state, actin-activated ATPase assays showed no change in either K_M or V_{MAX} value when actin was decorated with tropomyosin (Hodges *et al.*, 2012). For this myosin, duty cycle was increased by slowing the rate of ADP release and the rate of ATP-induced dissociation of the acto-motor complex (Hodges *et al.*, 2012). The effects of tropomyosin on P_i release rate were not as pronounced as they were for Myo52p.

Alternative modes of Cdc8p regulation and their relationship to established models

Myo52p was capable of processive movements on bare actin at low ATP. This condition increases motor duty ratio because ATP

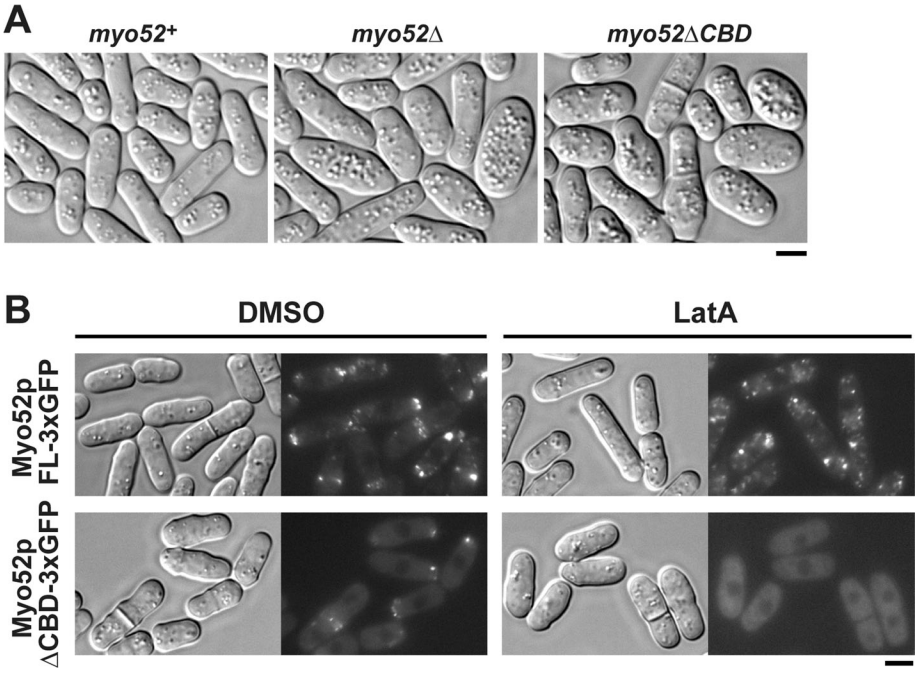

FIGURE 5: The cargo-binding domain of Myo52p is essential for in vivo function and clustering of Myo52p in subcellular particles in the absence of actin. (A) Wild-type and *myo52* mutant strains were grown at 32°C in YE5S rich media before microscopic imaging. Representative differential interference contrast (DIC) images of wild-type *myo52*$^{+}$ (*myo52-3xGFP*) cells (left), *myo52* null mutants (center), and the truncation mutant (*myo52ΔCBD-3xGFP*, right), which lacks sequence encoding the C-terminal cargo-binding domain (amino acids 1025–1516). Both mutants show a characteristic loss-of-function phenotype reflected by defects in cell shape (Motegi *et al.*, 2001; Win *et al.*, 2001). (B) Wild-type (*myo52-3xGFP*) and mutant (*myo52ΔCBD-3xGFP*) cells were grown at 25°C in YE5S rich media before imaging. Representative DIC and fluorescence micrographs show the subcellular localization of full-length Myo52p-3xGFP (top) and Myo52pΔCBD-3xGFP (bottom) upon treatment with dimethylsulfoxide (controls, left) or 10 μM latrunculin A (right). Bars, 4 μm.

binding becomes rate limiting, so that myosin motors spend most of their time without nucleotide in the strong actin-bound rigor state. The ability of bare actin to support processivity is consistent with a general mechanism in which tropomyosin mediates processivity by increasing the duty ratio, as opposed to changing the structure of the actin track. Strikingly, the frequency at which Myo52p processivity was observed at low ATP was sevenfold higher when actin was decorated with Cdc8p. The decreased K_M value (higher affinity) seen in the presence of tropomyosin in ATPase assays (Clayton *et al.*, 2010) may account for this increase in run frequency. In addition, as with *Sc* Myo2p and budding yeast Tpm1p, the average Myo52p run length increased at low ATP in the presence of Cdc8p. This was unexpected, given that the predicted duty ratio would be >95% whether tropomyosin is present or not. One possibility to explain the enhanced run length is improved gating between the two heads, perhaps by slowing ADP release from the lead head, as previously suggested for *Sc* Myo2p (Hodges *et al.*, 2012). Meanwhile, recent structural evidence suggests a more direct role for tropomyosin in myosin recruitment. A pseudoatomic model of a rigor motor head actin-tropomyosin complex, based on an 8-Å structure determined by cryo–electron microscopy, showed for the first time a direct interaction between myosin and tropomyosin in the actin-bound complex (Behrmann *et al.*, 2012). Collectively these findings suggest that tropomyosin promotes processivity by doing more than simply increasing the duty cycle of the motor.

A related mechanism, which can also apply to multiple motors, may lie in cooperative binding of myosin heads. Such a mechanism is a variation on the role of tropomyosin in striated muscle contraction, where the troponin-tropomyosin complex establishes a "blocked" state on the actin filament that prevents myosin-II binding (Lehrer, 1994; Swartz *et al.*, 1996; Gordon *et al.*, 2000). Binding of Ca^{2+} to troponin triggers a shift in the position of tropomyosin from the "blocked" to "closed" state. The "closed" state is initially inhibitory, as it requires binding of a myosin head to complete the shift in tropomyosin position to the "open" state, which then allows unrestricted and cooperative binding of neighboring myosin heads. The high concentrations of actin and myosin in muscle, coupled with the precise manner in which these molecules are lined up in sarcomeres, favors rapid movement into the "open" state.

Cryo–electron microscopy showed that Cdc8p-decorated actin filaments assume the "closed" state (Skoumpla *et al.*, 2007), which predictably results in inhibition of skeletal muscle myosin-II actin-activated ATPase activity (East *et al.*, 2011). However, these same Cdc8p-actin filaments significantly enhance *Sp* Myo2p and Myo52p activity in the same assays (Clayton *et al.*, 2010; Stark *et al.*, 2010). Enhancement of Myo52p activity by Cdc8p does not appear to be limited by the "closed" state, given that very low concentrations of Myo52p (<1 nM) were able to walk on Cdc8p-decorated filaments in single-molecule assays. Moreover, the actin-dependent clustering of truncated Myo52p motors lacking cargo that we observed on actin cables in vivo is reminiscent of cooperative binding, in which binding of one head favors the binding of neighboring heads close by.

We propose that the "closed" state is multifaceted and can activate (e.g., Myo52p with Cdc8p), inhibit (e.g., skeletal muscle myosin-II with Cdc8p), or block (e.g., fission yeast myosin-I with Cdc8p) motor activity, depending on the tropomyosin and myosin isoforms in play. In the case of Myo52p and Cdc8p, the "closed" state may favor activation by promoting initial actomyosin interactions that subsequently influence the position of Cdc8p and favor more interactions. However, this same state can completely block or limit initial interactions with muscle myosin needed for any subsequent cooperative binding. Activation of Myo52p by Cdc8p may reflect kinetic regulation in combination with cooperative effects by which the strong binding of one head shifts the position of tropomyosin, thus favoring strong binding of additional heads nearby.

MATERIALS AND METHODS

Fission yeast strains and genetic approaches

Standard fission yeast genetic and cell biology protocols were used (Moreno *et al.*, 1991). *myo52Δ::nat*^{R} (h^{-}, MLY 759), *myo52-3xGFP:kan*^{R} (h^{-}, MLY 975), *myo52ΔCBD-3xGFP:kan*^{R} (h^{+}, LP 86), and *clc1-3xGFP: kan*^{R} *uch2-mCherry:nat*^{R} (h^{+}, LP 123) haploid strains were constructed by performing genomic integrations using the relevant G418-resistant (*kan*^{R}) or nourthreothricin-resistant

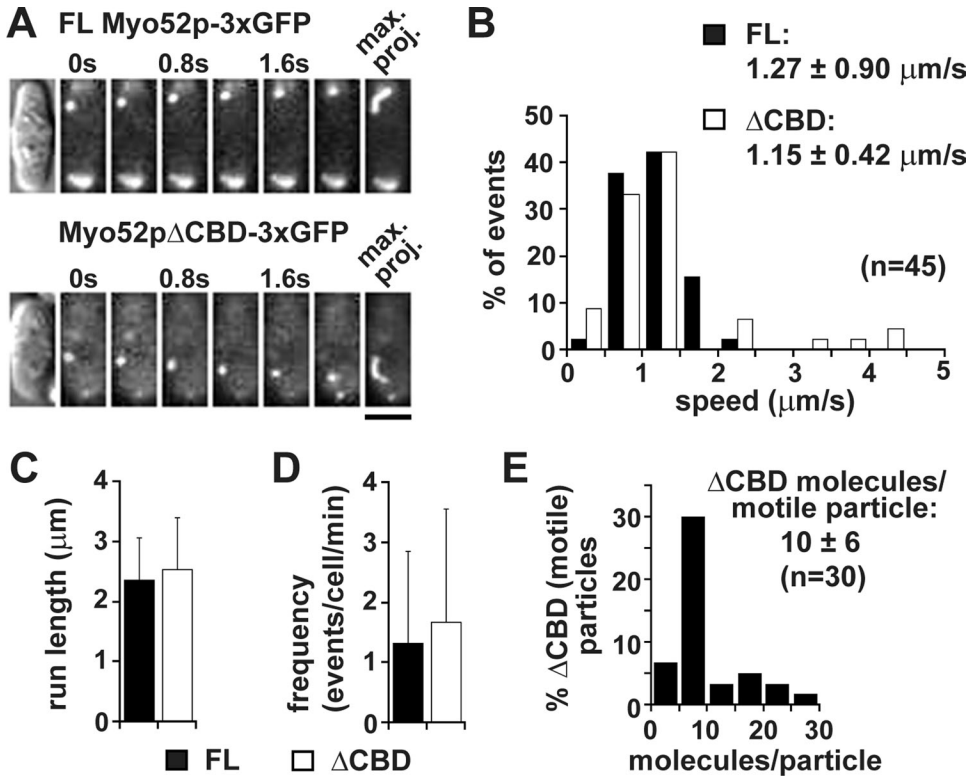

FIGURE 6: Myo52p molecules lacking their cargo-binding domain undergo efficient motility along actin cables. (A) Time-lapse montages showing directed movement of full-length Myo52p-3xGFP (top) and truncated Myo52pΔCBD-3xGFP (bottom) particles in wild-type *myo52-3xGFP* and *myo52ΔCBD-3xGFP* cells, respectively (after growth on YE5S rich medium at 25°C). Directed movements were captured over time using TIRF microscopy. Far right, maximum projections of the particle trajectories. Bar, 4 μm. Representative events from the *myo52ΔCBD-3xGFP* strain are also presented in Supplemental Movie S5. (B) Histogram of the speed distribution of full-length Myo52p and Myo52pΔCBD particles. (C, D) Average run length ($n = 45$ in C) and event frequency (cell number = 82–122 in D) of motile Myo52p and Myo52pΔCBD particles. (E) Histogram of Myo52pΔCBD GFP intensity as number of dimeric motors/motile particle.

(*nat*^{R}) antibiotic markers and (YE5S-drug) rich media selection plates (Bahler *et al.*, 1998; Snaith *et al.*, 2010). The *myo52ΔCBD-3xGFP* strain encodes a C-terminal truncation in which the globular cargo-binding region of the Myo52p tail (amino acids 1025–1516) is replaced by a triple-GFP tag. The SFY 527/528 strain background (h$^-$/h$^+$ *leu1-32 ura4-D18 his3-D1 ade6-M216/ade6-M210*) was used throughout. An exception was the *myo52ΔCBD-tdTomato* strain, which was a gift from Sophie Martin (University of Lausanne, Lausanne, Switzerland; Lo Presti *et al.*, 2012).

Plasmids

A PCR product encoding a truncated form of Myo52p (amino acids 1–1056 spanning the motor domain, light chain–binding region, and coiled-coil region) was amplified from *S. pombe* cDNA. The fragment was cloned into the baculovirus transfer vector pAcSG2 with a C-terminal biotin tag, followed by a C-terminal FLAG tag for purification by affinity chromatography. The biotin tag is an 88–amino acid sequence segment from the *Escherichia coli* biotin carboxyl carrier protein, which, when expressed in Sf9 cells, is biotinylated at a single Lys residue. The tag is used for attachment to streptavidin-coated Qdots or streptavidin-Cy3. Myo52p light-chain genes (*cam1* and *cdc4*) were amplified from *S. pombe* cDNA and cloned into the dual expression vector pAcUW51 behind separate promoters. The fidelity of constructs was confirmed by DNA sequencing.

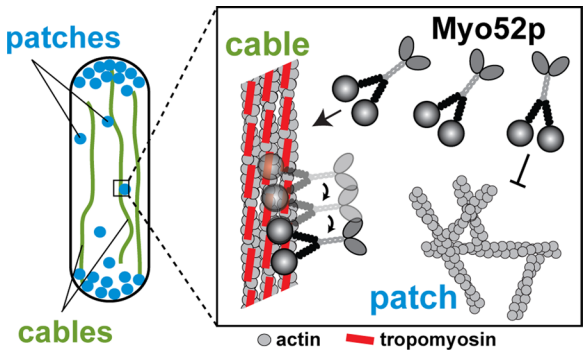

FIGURE 7: Sorting of Myo52p to actin cables during interphase. An interphase cell uses two distinct actin structures: 1) endocytic actin patches (blue) made up of branched actin filament networks that associate with myosin-I (Myo1p) and lack tropomyosin (Cdc8p), and 2) actin cables (green) made up of unbranched polarized Cdc8p-decorated actin filaments that support Myo52p transport throughout the cell cycle (Kovar *et al.*, 2011). Box, the presence of Cdc8p on actin cables facilitates Myo52p interactions by converting cytoplasmic Myo52p molecules into processive motors, which preferentially bind to and move efficiently along the cables. The absence of tropomyosin at actin patches fails to support Myo52p processivity, preventing inappropriate interactions between myosin-V and endocytic actin structures.

A Cdc8p construct was used to overexpress an acetylated-mimicking form of the protein in *E. coli*. The *cdc8* gene was PCR amplified from *S. pombe* cDNA using the following primers: 5′, *Nde*I-*cdc8*, CAAT*CATATG*GCTAGCATGGATAAGCTTAGAGAG (the *Nde*I site is italicized, and the start codon of the *cdc8* ORF is underlined); and 3′, *Bam*HI-*cdc8* CAAT*GGATCC*CTACAAGTCCTCA-AGAGCTT (the *Bam*HI site is italicized, and the *cdc8* stop codon is underlined). The 5′ primer encodes an Ala-Ser (acetylation mimicking) dipeptide immediately upstream of the *cdc8* start codon. The start codon for the recombinant protein actually lies in the second half of the *Nde*I site, allowing for incorporation of the Ala-Ser codons. The resultant oligonucleotide was cloned into the pET3 vector and fidelity confirmed by DNA sequencing.

The *cam1* and *cdc4* Myo52p light-chain open reading frames were cut out from the pAcUW51 baculovirus vector using *Bam*HI and inserted into the *Bam*HI sites of pET3a for bacterial expression. The orientation and fidelity of the light-chain sequences was confirmed by restriction analysis and DNA sequencing.

The *pREP41-tdTomato-ypt3* plasmid was a gift from Sophie Martin (Lo Presti and Martin, 2011) and was used to visualize Myo52p-dependent localization of Ypt3p at polarized growth sites (Supplemental Figure S3).

Live-cell imaging

Tracking of Myo52p-3xGFP particle motility used a Nikon (Melville, NY) Eclipse Ti-U inverted microscope equipped with a 100× PlanApo objective lens (1.40 numerical aperture [NA]) for through-the-objective near-TIRF microscopy. The GFP was excited with a 473-nm laser line. The angle at which the laser entered the objective was tuned such that the illumination was not perfect TIRF, allowing the laser to excite the entire thickness of the cell, yet resulting in a better signal-to-noise ratio than with epi-illumination. Images were obtained using a Stanford Photonics XR/Turbo-Z camera running Piper Control (Stanford, CA) version 2.3.39, software. The pixel resolution was 145.5 nm. Data were collected at 7.7 frames/sat room temperature. Movement of GFP particles over time was tracked manually using ImageJ (National Institutes of Health, Bethesda, MD).

A Nikon TE2000-E2 inverted microscope with motorized fluorescence filter turret and a Plan Apo 60× (1.45 NA) objective was used to capture differential interference contrast and epifluorescence images (using GFP or tetramethyl rhodamine isothiocyanate filters) at room temperature. Fluorescence used an EXFO X-CITE 120 illuminator (Mississauga, Ontario, Canada). NIS Elements software (Melville, NY) was used to control the microscope, together with two Uniblitz shutters (Rochester, NY). A Photometrics (Tucson, AZ) CoolSNAP HQ2 14-bit camera was used for single-plane colocalization imaging of Myo52p-3xGFP (or Myo52pΔCBD-3xGFP) and Tomato-Ypt3p (Supplemental Figure S2). Time-lapse movies of cells monitoring Clc1p-3xGFP patches and Myo52p-3xGFP (or Myo52pΔCBD-3xGFP) particles were captured using an Andor (Belfast, UK) 16-bit electron-multiplying charge-coupled device camera. Images were captured every 2 s as *z*-stacks (every 0.70 µm over 4.2 µm) spanning the cell depth.

Cell suspensions (3 µl) were mounted on flat, 30-µl media pads (solidified by 1% agarose) prepared on the slide surface. VALAP (1:1:1 Vasoline, lanolin, and paraffin) was used to seal slides and coverslips. Latrunculin A treatment (10 µM) was used to remove actin cables from *myo52-3xGFP* and *myo52ΔCBD-3xGFP* cells growing exponentially in YE5S media. Images were captured 45 min after the addition of the drug (or dimethylsulfoxide in controls).

Protein purification

Myo52p-HMM. Baculovirus harboring the Myo52p and Cam1p-Cdc4p constructs was prepared using established protocols (Hodges *et al.*, 2009). Sf9 cells were coinfected with both the heavy and light chains. Sf9 cells were grown in suspension and harvested at 72 h. Harvested cells were pelleted at low speed for 10 min and resuspended in lysis buffer (300 mM NaCl, 10 mM imidazole, pH 7.2, 1 mM ethylene glycol tetraacetic acid [EGTA], 5 mM $MgCl_2$, 2 mM dithiothreitol [DTT], 5 µg/ml leupeptin, 0.8 mg/ml benzamidine, and 0.4 µg/ml recombinant Cam1p and Cdc4p). Cells were lysed by sonication and pelleted after addition of 2 mM Mg^{2+}-ATP. The supernatant was incubated with anti-FLAG resin for 1.5 h, transferred to a column, and washed with 100 ml of FLAG buffer (300 mM NaCl, 10 mM imidazole, pH 7.2, 1 mM EGTA, 1 mM NaN_3). The sample was eluted off the column by the addition of FLAG buffer containing 150 µg/ml FLAG peptide. Protein-rich fractions were pooled followed by three rounds of dialysis (3 × 1 l) against storage buffer (300 mM KCl, 10 mM imidazole, pH 7.2, 1 mM NaN_3, 1 mM DTT), followed by addition of 5 µg/ml leupeptin.

Cdc8p and Myo52p light-chain proteins were produced in *E. coli* BL21 DE3–competent cells. Cultures were grown in LB media at 37°C and protein overexpression induced at an OD_{600} of 0.5 by addition of 0.4 mM isopropyl-β-D-thiogalactoside. Cells were harvested after overnight induction at 25°C. Proteins were purified as described previously (Pruyne *et al.*, 1998). Cell pellets were resuspended in lysis buffer (100 mM NaCl, 10 mM imidazole, pH 7.2, 2 mM EDTA, and 1 mM DTT) and sonicated. Lysates were boiled for 10 min while stirring, then pelleted to remove denatured protein and other debris. Soluble tropomyosin (or light chains) were precipitated from the supernatant by lowering the pH to 0.2 U below the isoelectric point of the relevant protein. The protein precipitate was resuspended in 50 mM NaCl, 1 mM DTT, and 10 mM imidazole, pH 7.4, and dialyzed for three rounds (3 × 1 l) against the same buffer, followed by addition of 5 µg/ml leupeptin.

Chicken skeletal muscle proteins. Actin was purified from acetone powder (Spudich and Watt, 1971), and myosin-II was purified as described previously (Margossian and Lowey, 1982).

Visualizing Myo52p-Qdot and Myo52p-Cy3 motility by TIRF microscopy

Myo52p-HMM (0.2 µM) was mixed with a twofold molar excess of actin and 2 mM Mg^{2+}-ATP and centrifuged for 20 min at 400,000 × *g* to remove any myosin that was unable to dissociate from actin in the presence of ATP. To investigate processivity of individual myosin V motors, Myo52p was then mixed with a 10-fold molar excess of 655-nm streptavidin-coated Qdots (Invitrogen, Grand Island, NY). In principle, a small fraction of Qdots will have two or more motors bound, but previous controls demonstrated that Qdots are driven primarily by a single motor at this mixing ratio (Hodges *et al.*, 2012). To investigate multiple motor transport, we mixed Qdots with a 10-fold excess of Myo52p to generate Qdots with multiple motors, with typical saturation yielding ~3–5 motors/Qdot based on geometrical considerations (Hodges *et al.*, 2009, 2012). Flow cells made from glass coverslips were prepared by introducing the following solutions into the flow cell: 0.1 mg/ml *N*-ethylmaleimide–modified skeletal muscle myosin (5-min incubation), 5× rinse of 1 mg/ml bovine serum albumin (BSA; 2 min), 2 µM rhodamine-phalloidin–labeled chicken skeletal muscle actin filaments (plus or minus 1 µM tropomyosin; 2–5 min), 5× rinse with motility buffer, and, finally 0.2 nM Myo52p in motility buffer with 2 mM MgATP. Motility buffer consists of 50 mM KCl, 25 mM imidazole, pH 7.4, 4 mM $MgCl_2$,

1 mM EGTA, 50 mM DTT, 1 mg/ml BSA, 3.5 μM fission yeast calmodulin (Cam1p), 3.5 μM fission yeast essential light chain (Cdc4p), and an oxygen-scavenging system (3 mg/ml glucose, 0.1 mg/ml glucose oxidase, and 0.18 mg/ml catalase). For experiments with Cdc8p, 1 μM Cdc8p was included in the motility buffer to prevent dissociation from actin.

For single-molecule experiments using Cy3-labeled Myo52p, motors were mixed with a fivefold molar excess of Cy3-streptavidin (Invitrogen) and diluted to a final concentration of 0.5 nM in buffer C-50 (10 mM imidazole, pH 7.4, 50 mM KCl, 4 mM $MgCl_2$, 1 mM EGTA, 10 mM DTT, plus light chains, oxygen scavengers, and 2 μM Cdc8p when included) before adding to the flow cell. Alexa 635-phalloidin–labeled chicken skeletal muscle actin filaments were used.

Through-the-objective TIRF microscopy was performed at room temperature using the Nikon Eclipse Ti-U microscope equipped with a 100× Plan Apo objective lens (1.49 NA) and auxiliary 1.5× magnification. Fluorophores were excited with a 473-nm (Qdots) or 532-nm (Cy3 and actin) laser line, and images were obtained using the XR/Turbo-Z camera running Piper Control software, version 2.3.39. The pixel resolution was 95.0 nm, and data were collected at 5–30 frames/s. Qdot movement along rhodamine-labeled actin filaments was tracked by hand using ImageJ. For each event, we required Qdot-labeled Myo52p to move continuously for at least three frames to qualify as a run. Cy3 movement along Alexa 635–labeled actin filaments was tracked using the MtrackJ plug-in for ImageJ. Runs that artificially terminated by running off the end of an actin filament were not included in the run length analysis.

ACKNOWLEDGMENTS

We thank Sophie Martin (University of Lausanne, Lausanne, Switzerland) for the *ypt3* plasmid and the *myo52ΔCBD-tdTomato* strain. We are very grateful to Guy Kennedy and David Warshaw (University of Vermont, Burlington, VT) for providing access to and guidance with TIRF microscopy. This work was supported by American Heart Association Scientist Development Grant 0835236N and National Institutes of Health Grant GM097193 to M.L. and National Institutes of Health Grant GM078097 to K.M.T.

REFERENCES

Arai R, Nakano K, Mabuchi I (1998). Subcellular localization and possible function of actin, tropomyosin and actin-related protein 3 (Arp3) in the fission yeast *Schizosaccharomyces pombe*. Eur J Cell Biol 76, 288–295.

Bahler J, Wu JQ, Longtine MS, Shah NG, McKenzie A3rd, Steever AB, Wach A, Philippsen P, Pringle JR (1998). Heterologous modules for efficient and versatile PCR-based gene targeting in *Schizosaccharomyces pombe*. Yeast 14, 943–951.

Balasubramanian MK, Helfman DM, Hemmingsen SM (1992). A new tropomyosin essential for cytokinesis in the fission yeast *S. pombe*. Nature 360, 84–87.

Behrmann E, Muller M, Penczek PA, Mannherz HG, Manstein DJ, Raunser S (2012). Structure of the rigor actin-tropomyosin-myosin complex. Cell 150, 327–338.

Clayton JE, Sammons MR, Stark BC, Hodges AR, Lord M (2010). Differential regulation of unconventional fission yeast myosins via the actin track. Curr Biol 20, 1423–1431.

Collins K, Sellers JR, Matsudaira P (1990). Calmodulin dissociation regulates brush border myosin I (110-kD-calmodulin) mechanochemical activity in vitro. J Cell Biol 110, 1137–1147.

Cooper JA (2002). Actin dynamics: tropomyosin provides stability. Curr Biol 12, R523–R525.

De La Cruz EM, Wells AL, Rosenfeld SS, Ostap EM, Sweeney HL (1999). The kinetic mechanism of myosin V. Proc Natl Acad Sci USA 96, 13726–13731.

East DA, Sousa D, Martin SR, Edwards TA, Lehman W, Mulvihill DP (2011). Altering the stability of the Cdc8 overlap region modulates the ability of this tropomyosin to bind co-operatively to actin and regulate myosin. Biochem J 438, 265–273.

Edamatsu M, Toyoshima YY (2003). Fission yeast synaptobrevin is involved in cytokinesis and cell elongation. Biochem Biophys Res Commun 301, 641–645.

Fanning AS, Wolenski JS, Mooseker MS, Izant JG (1994). Differential regulation of skeletal muscle myosin-II and brush border myosin-I enzymology and mechanochemistry by bacterially produced tropomyosin isoforms. Cell Motil Cytoskeleton 29, 29–45.

Gordon AM, Homsher E, Regnier M (2000). Regulation of contraction in striated muscle. Physiol Rev 80, 853–924.

Grallert A, Martin-Garcia R, Bagley S, Mulvihill DP (2007). In vivo movement of the type V myosin Myo52 requires dimerisation but is independent of the neck domain. J Cell Sci 120, 4093–4098.

Gunning PW, Schevzov G, Kee AJ, Hardeman EC (2005). Tropomyosin isoforms: divining rods for actin cytoskeleton function. Trends Cell Biol 15, 333–341.

Hodges AR, Bookwalter CS, Krementsova EB, Trybus KM (2009). A nonprocessive class V myosin drives cargo processively when a kinesin-related protein is a passenger. Curr Biol 19, 2121–2125.

Hodges AR, Krementsova EB, Bookwalter CS, Fagnant PM, Sladewski TE, Trybus KM (2012). Tropomyosin is essential for processive movement of a class V myosin from budding yeast. Curr Biol 22, 1410–1416.

Kovar DR, Sirotkin V, Lord M (2011). Three's company: the fission yeast actin cytoskeleton. Trends Cell Biol 21, 177–187.

Lehrer SS (1994). The regulatory switch of the muscle thin filament: Ca2+ or myosin heads? J Muscle Res Cell Motil 15, 232–236.

Lo Presti L, Chang F, Martin SG (2012). Myosin Vs organize actin cables in fission yeast. Mol Biol Cell 23, 4579–4591.

Lo Presti L, Martin SG (2011). Shaping fission yeast cells by rerouting actin-based transport on microtubules. Curr Biol 21, 2064–2069.

Margossian SS, Lowey S (1982). Preparation of myosin and its subfragments from rabbit skeletal muscle. Methods Enzymol 85, B55–71.

Martin-Garcia R, Mulvihill DP (2009). Myosin V spatially regulates microtubule dynamics and promotes the ubiquitin-dependent degradation of the fission yeast CLIP-170 homologue, Tip1. J Cell Sci 122, 3862–3872.

Martin-Garcia R, Valdivieso MH (2006). The fission yeast Chs2 protein interacts with the type-II myosin Myo3p and is required for the integrity of the actomyosin ring. J Cell Sci 119, 2768–2779.

Mehta AD, Rock RS, Rief M, Spudich JA, Mooseker MS, Cheney RE (1999). Myosin-V is a processive actin-based motor. Nature 400, 590–593.

Merkel L, Ikebe M, Hartshorne DJ (1989). Interaction of smooth muscle tropomyosin and smooth muscle myosin. Effect on the properties of myosin. Biochemistry 28, 2215–2220.

Moreno S, Klar A, Nurse P (1991). Molecular genetic analysis of fission yeast *Schizosaccharomyces pombe*. Methods Enzymol 194, 795–823.

Motegi F, Arai R, Mabuchi I (2001). Identification of two type V myosins in fission yeast, one of which functions in polarized cell growth and moves rapidly in the cell. Mol Biol Cell 12, 1367–1380.

Mulvihill DP, Edwards SR, Hyams JS (2006). A critical role for the type V myosin, Myo52, in septum deposition and cell fission during cytokinesis in *Schizosaccharomyces pombe*. Cell Motil Cytoskeleton 63, 149–161.

Nosaka S, Onji T, Shibata N (1984). Enhancement of actomyosin ATPase activity by tropomyosin. Recombination of myosin and tropomyosin between muscles and platelet. Biochim Biophys Acta 788, 290–297.

Pruyne DW, Schott DH, Bretscher A (1998). Tropomyosin-containing actin cables direct the Myo2p-dependent polarized delivery of secretory vesicles in budding yeast. J Cell Biol 143, 1931–1945.

Reck-Peterson SL, Tyska MJ, Novick PJ, Mooseker MS (2001). The yeast class V myosins, Myo2p and Myo4p, are nonprocessive actin-based motors. J Cell Biol 153, 1121–1126.

Siemankowski RF, Wiseman MO, White HD (1985). ADP dissociation from actomyosin subfragment 1 is sufficiently slow to limit the unloaded shortening velocity in vertebrate muscle. Proc Natl Acad Sci USA 82, 658–662.

Sirotkin V, Berro J, Macmillan K, Zhao L, Pollard TD (2010). Quantitative analysis of the mechanism of endocytic actin patch assembly and disassembly in fission yeast. Mol Biol Cell 21, 2894–2904.

Skoumpla K, Coulton AT, Lehman W, Geeves MA, Mulvihill DP (2007). Acetylation regulates tropomyosin function in the fission yeast *Schizosaccharomyces pombe*. J Cell Sci 120, 1635–1645.

Snaith HA, Anders A, Samejima I, Sawin KE (2010). New and old reagents for fluorescent protein tagging of microtubules in fission yeast; experimental and critical evaluation. Methods Cell Biol 97, 147–172.

Snaith HA, Thompson J, Yates JR3rd, Sawin KE (2011). Characterization of Mug33 reveals complementary roles for actin cable-dependent

transport and exocyst regulators in fission yeast exocytosis. J Cell Sci 124, 2187–2199.
Spudich JA, Watt S (1971). The regulation of rabbit skeletal muscle contraction. I. Biochemical studies of the interaction of the tropomyosin-troponin complex with actin and the proteolytic fragments of myosin. J Biol Chem 246, 4866–4871.
Stark BC, Sladewski TE, Pollard LW, Lord M (2010). Tropomyosin and myosin-II cellular levels promote actomyosin ring assembly in fission yeast. Mol Biol Cell 21, 989–1000.
Swartz DR, Moss RL, Greaser ML (1996). Calcium alone does not fully activate the thin filament for S1 binding to rigor myofibrils. Biophys J 71, 1891–1904.
Takagi Y, Yang Y, Fujiwara I, Jacobs D, Cheney RE, Sellers JR, Kovacs M (2008). Human myosin Vc is a low duty ratio, nonprocessive molecular motor. J Biol Chem 283, 8527–8537.
Tang N, Ostap EM (2001). Motor domain-dependent localization of myo1b (myr-1). Curr Biol 11, 1131–1135.
Toth J, Kovacs M, Wang F, Nyitray L, Sellers JR (2005). Myosin V from *Drosophila* reveals diversity of motor mechanisms within the myosin V family. J Biol Chem 280, 30594–30603.
Warshaw DM, Kennedy GG, Work SS, Krementsova EB, Beck S, Trybus KM (2005). Differential labeling of myosin V heads with quantum dots allows direct visualization of hand-over-hand processivity. Biophys J 88, L30–32.
Watanabe S, Watanabe TM, Sato O, Awata J, Homma K, Umeki N, Higuchi H, Ikebe R, Ikebe M (2008). Human myosin Vc is a low duty ratio nonprocessive motor. J Biol Chem 283, 10581–10592.
Win TZ, Gachet Y, Mulvihill DP, May KM, Hyams JS (2001). Two type V myosins with non-overlapping functions in the fission yeast *Schizosaccharomyces pombe*: Myo52 is concerned with growth polarity and cytokinesis, Myo51 is a component of the cytokinetic actin ring. J Cell Sci 114, 69–79.
Yamaguchi M, Ver A, Carlos A, Seidel JC (1984). Modulation of the actin-activated adenosinetriphosphatase activity of myosin by tropomyosin from vascular and gizzard smooth muscles. Biochemistry 23, 774–779.